

<sup>1</sup> Cover Letter

<sup>2</sup> **A Fast Method for Detecting Rock Blocks and Calculating Volumes and 3D Surface Areas**

<sup>3</sup> Ali Polat

<sup>4</sup> Dear Editors-in-Chief,

<sup>5</sup>

<sup>6</sup> please find the enclosed manuscript "A Fast Method for Detecting Rock Blocks and Calculating Volumes and 3D Sur-  
<sup>7</sup> face Areas" which i am submitting for exclusive consideration for publication in Computers & Geosciences. I confirm  
<sup>8</sup> that the submission follows all the requirements and includes all the items of the submission checklist.

<sup>9</sup>

<sup>10</sup> The manuscript presents a fast method for detecting rock blocks. Rock blocks were detected precisely using the U-Net  
<sup>11</sup> network and transfer learning method. Train IoU, validation IoU, train F1-score and validation F1-score were calcu-  
<sup>12</sup> lated as 0.8497%, 0.8461%, 0.9186%, and 0.9152%, respectively. An algorithm was developed to calculate the volume  
<sup>13</sup> and 3D surface area of rock blocks. The methods and algorithms used in the study can be used in many fields, such as  
<sup>14</sup> engineering applications and geological-geomorphological studies.

<sup>15</sup>

<sup>16</sup> I provide the source codes in a public repository with details listed in the section "Code availability".

<sup>17</sup>

<sup>18</sup> Thanks for your consideration.

<sup>19</sup>

<sup>20</sup> Sincerely,

<sup>21</sup>

<sup>22</sup> Ali Polat

<sup>23</sup> Provincial Directorate of Disaster and Emergency, 58000, Sivas, Turkey ali.polat@afad.gov.tr

<sup>24</sup>

<sup>25</sup> **Delete before submission:**

<sup>26</sup> Please confirm that your submission follows all the requirements of the guidelines, including the submission checklist:

<sup>27</sup> - Cover letter

<sup>28</sup> - Highlights

<sup>29</sup> - Authorship statement

<sup>30</sup> - The manuscript must be single column and double spaced

<sup>31</sup> - Reference must be in the author-date format

<sup>32</sup> - Code availability section

<sup>33</sup> \*The manuscripts that do not meet the requirement guidelines will be desk-rejected.

34 **Highlights**

35 **A Fast Method for Detecting Rock Blocks and Calculating Volumes and 3D Surface Areas**

36 Ali Polat

- 37
- Rock blocks were detected precisely using the U-Net network and transfer learning method.

38

  - An algorithm was developed to calculate the volume and 3D surface area of rock blocks.

39

  - The approach can be readily adapted to other terrain-related segmentation problems, as well as to the calculation of volume and 3D surface areas.

40

# 41 A Fast Method for Detecting Rock Blocks and Calculating Volumes 42 and 3D Surface Areas

43 Ali Polat

44 Provincial Directorate of Disaster and Emergency, 58000, Sivas, Turkey

45

---

## 46 ARTICLE INFO

47

48 **Keywords:**

49 Rock segmentation

50 U-Net

51 Convolutional Neural Networks

52 Rockfall

53 Volume Calculation

54 3D Surface Area Calculation

55

56

57

58

59

60

61

62

63

64

65

66

67

---

## 68 1. Introduction

69 In many parts of the world, loss of life and property is experienced, and large-scale economic losses occur due to  
70 natural disasters. One of these natural disasters is rockfall events. Rockfalls are a type of slope instability in which  
71 blocks of rock confined to discontinuities move very rapidly from the source region (Varnes, 1978; Hutchinson, 1988;  
72 Cruden and Varnes, 1996). Due to the high velocity during the event, rockfalls can be very dangerous for structures  
73 in their route depending on the block size. Although it is a type of disaster that affects small areas, its consequences  
74 can be very serious. That's why rockfall prevention studies are important. There are also studies on this subject in  
75 the literature (Liu et al., 2021; Keskin and Polat, 2022; Ji et al., 2023; Kainthola et al., 2023; Cao et al., 2024). Some  
76 preliminary studies are needed to develop a prevention method. One of them is the detection of rock blocks and the  
77 calculation of their geometric properties. In this study, rock blocks were segmented, and their volumes and 3D surface  
78 areas were calculated. There are various studies on rock segmentation in the literature.

79 In 2006, Dunlop (Dunlop, 2006) developed a technique for characterization of rocks using albedo, colour, tex-  
80 ture and shape features. In that work rocks in natural scenes are segmented and located with an accurate boundary.  
81 For segmentation purpose top-down and bottom-up knowledge are combined, and geologic rock analysis performed

---

ORCID(s): 0000-0002-9147-3633 (A. Polat)

82 successfully.

83 In the study carried out by Song (Song and Shan, 2006) in this area in 2006, segmentation studies of rocks on  
84 Mars were carried out in order to plan the route and determine the landing areas. Texture-based image segmentation  
85 and edge-flow driven active contour has been developed. Wavelet based local transform, multi-resolution histograms,  
86 and inter-scale decision were combined and used for rock segmentation. As a result of the experiments, reliable rock  
87 segmentation results were obtained by Song.

88 The place of visual navigation in planetary rover autonomy is crucial. Rock segmentation is an important and  
89 challenging task for rover autonomy due to the high computational load and real-time requirement. Kuang et al.  
90 (Kuang et al., 2021) propose a rock segmentation network (NI-U-Net++) to aid in the visual navigation of rovers. The  
91 created model consists of two stages. In the first step, called pre-training, synthetic rock images are created and then  
92 the generated images are used to pre-train the NI-U-Net++ network. The second phase, transfer-training, fine-tunes  
93 the pre-trained NI-U-Net++ network with real-life images.

94 Guo et al. (Guo et al., 2022) proposed an adaptive watershed segmentation method based on distance transformation  
95 for blasted rock piles images. They obtained 95.65% segmentation accuracy for limestone and granite rock blocks with  
96 area over 100 cm<sup>2</sup>.

97 Segmentation of rocks is important in mining as well as in geology. Segmentation is used in this area to deter-  
98 mine the size distribution of rock fragments, to organize and optimize blasting, and to reduce environmental impact.  
99 For this purpose, Malladi et al. (Malladi et al., 2014) proposed a simple superpixel algorithm called Superpixels Us-  
100 ing Morphology (SUM), which uses a watershed transformation approach to generate superpixels; and made a study  
101 comparing some of the current superpixel algorithms on rock images.

102 Recently, various deep learning and machine learning algorithms, including Convolutional Neural Networks (CNN),  
103 have been proposed by researchers working on rock segmentation. Karimpouli and Tahmasebi (Karimpouli and Tah-  
104 masebi, 2019) used convolutional autoencoder networks called SegNet for segmentation of digital rock images. Due to  
105 the limited number of rock images, cross-correlation based simulation was applied to increase the number of images.  
106 20 images taken from Berea sandstone were used as dataset. As a result of the tests, they obtained an accuracy value  
107 of 96

108 Xue et al. (Xue et al., 2021) made rock segmentation study for a different purpose; they proposed the rock seg-  
109 mentation visual system to assist Tunnel Boring Machine (TBM) driving. TBM is an essential equipment for digging  
110 long-range tunnels. They applied different deep learning network for semantic segmentation of rocks.

111 In the above studies, rock segmentation was carried out for different purposes. In this study, rock segmentation  
112 was carried out as a necessary preliminary study in the development of rockfall prevention methods. Rock blocks were  
113 detected precisely in a fast, economical and safe way. In addition, the volumes and 3D surface areas of rock blocks were

<sup>114</sup> calculated. The methods and algorithms used in the study can be used in many fields such as engineering applications,  
<sup>115</sup> and geological-geomorphological studies.

<sup>116</sup> **1.1. Study area**

<sup>117</sup> The study area is in the north of Karasar village, which is approximately 156 km away from Sivas city (Fig. 1).  
<sup>118</sup> This area consists of Middle Miocene aged agglomerate and tuff units (MTA 1/25000) (Fig. 2). This unit was defined  
<sup>119</sup> as Adatepe volcanites according to (Yilmaz and Yilmaz, 2004). The unit consists of black, red-brown, and brown-  
<sup>120</sup> black colored basaltic lava flows and less commonly agglomerate and tuffs. The rock blocks in this unit expose a risk  
<sup>121</sup> of rockfall. Lower Miocene aged sandstone-mudstone-limestone units are observed in the settlement area (Karasar  
<sup>122</sup> village) and vicinity.

<sup>123</sup> Karasar village is located on the slopes of a hill. The bedrock on the hill is heavily fractured and cracked. There  
<sup>124</sup> are many rock blocks that have fallen from the upper parts of the slope. The sizes of these blocks vary from  $0.5 m^3$  to  
<sup>125</sup>  $15 m^3$ . Rapid temperature changes, heavy snow and precipitation, freeze-thaw, earthquake, and human-induced causes  
<sup>126</sup> increase the risk of rockfall in the region.

<sup>127</sup> **2. Methodology**

<sup>128</sup> Creating the dataset is a big problem for classification or segmentation processes. In this study, Unmanned Air  
<sup>129</sup> Vehicle (UAV) was used to collect data. An orthophoto image of the region was created from aerial photographs  
<sup>130</sup> obtained by UAV. An area was selected to create train images. Rock blocks within this area were labelled and mask  
<sup>131</sup> images were created. Then segmentation process was completed by Python and necessary libraries, and the results  
<sup>132</sup> were converted to the polygon as a vector file (Fig. 3). Moreover, the volumes of all the rocks were calculated. This  
<sup>133</sup> section includes an example of equation.

<sup>134</sup> **2.1. Data preparation**

<sup>135</sup> In this study required data was collected by UAV. DJI phantom 3-Pro was used for image acquisition. First, the  
<sup>136</sup> area to be flown is determined, then the necessary parameters for image acquisition are entered by the Pix4d Capture  
<sup>137</sup> software. These parameters were chosen as follows.

- <sup>138</sup> – Flight altitude (altitude): 100 m.
- <sup>139</sup> – Flight speed (speed): Fast
- <sup>140</sup> – Camera angle (Angle):  $70^\circ$
- <sup>141</sup> – Overlap: 80%

<sup>142</sup>  
<sup>143</sup> The flight was carried out by the "Double Grid" method. The model of UAV used in this study does not have an

144 obstacle detecting feature. Therefore, when determining the height, it is necessary to pay attention to the nearby power  
 145 lines, tall buildings, trees, and peaks of hills.

146 The camera model (FC00X) of UAV has 4000x3000 resolution, 3.61 mm focal length and 1.56 x 1.56  $\mu\text{m}$  pixel  
 147 dimensions. After the flight, 284 images were obtained, and these images were processed with the Pix4Dmapper  
 148 software. As a result, an orthophoto image with a resolution of 3.51 cm/pixel and a dimension of 2329x1587 was  
 149 created.

150 An area was selected to create train and test images from large orthophoto image. This area was selected randomly.  
 151 Then all rocks seen on the image were drawn on by GIS software. This file was saved as a vector file, and it will be  
 152 used as mask data in segmentation processes. After this process, we have created the image and mask files. A deep  
 153 learning model requires the same sizes of images. That's why a single image needs to be split into patches. The patch  
 154 dimension was used as 256x256. Train-test splitting size was selected as 66% for training data and 34% for testing  
 155 data. The large image was split into 9 part to avoid sampling from the same regions. Areas 1,5,9 were selected for  
 156 creating test images. Train images were selected from the others (2,3,4,6,7,8) areas (Fig. 4). A total of 600 images  
 157 (256x256) were selected, 369 images for training and 191 images for testing. The same processes were applied to  
 158 extract the mask images.

159 We also used the Albumentations (Buslaev et al., 2020) method for data augmentation during the model-building  
 160 stage. Albumentations includes many transform methods. We applied augmentation methods given below:

- 161 – horizontal flip
- 162 – affine transforms
- 163 – perspective transforms
- 164 – brightness/contrast/colours manipulations
- 165 – image blurring and sharpening
- 166 – gaussian noise

167

## 168 2.2. Model building

169 In this study, U-Net architecture (Ronneberger et al., 2015) was used as a segmentation model. This architecture  
 170 is a type of fully convolutional network developed for biomedical image segmentation. It is named U-Net because the  
 171 shape of the architecture is like the letter U. The network architecture of U-Net is shown in Figure 5. It consists of two  
 172 parts. These are the contracting path (left side) and expanding path (right side). The first part captures context, and the  
 173 second part enables precise localization. The left side consists of 4 blocks and each block contains two 3x3 convolution  
 174 layers + activation function (with batch normalization) and one 2x2 max-pooling layer. Also, the right side consists of

175 4 blocks. These blocks include the steps of deconvolution layer, merging with feature map from subsampling path, 3x3  
 176 convolution layer + activation function (with batch normalization). Finally, an additional 1x1 convolution operation  
 177 is applied to reduce the feature map to the required number of channels and generate the segmented image.

178 DenseNet121 transfer learning models were used for feature extraction and rock segmentation was performed with  
 179 U-Net. Segmentation model was evaluated in terms of Intersection over Union (IoU) and f1-score metrics. For the  
 180 calculate loss value dice loss was used. IoU, which is frequently preferred in segmentation problems, is also known as  
 181 the Jaccard similarity coefficient (Jaccard, 1912). It is the ratio of correctly classified pixels to the sum of the number  
 182 of pixels in that class and the predicted number of pixels. Mean IoU is the average IoU of all classes and presented in  
 183 equation 1.

$$J(A, B) = \frac{|A \cap B|}{|A \cup B|} \quad (1)$$

184 The F1-Score is important in that it is not False Negative or False Positive, but a measurement metric that includes all  
 185 error costs. It is the harmonic mean of Precision and Recall values (Equation 2).

$$F1\text{-Score} = \frac{2 \times \text{Precision} \times \text{Recall}}{\text{Precision} + \text{Recall}} \quad (2)$$

$$\text{Precision} = \frac{TP}{TP + FP}$$

$$\text{Recall} = \frac{TP}{TP + FN}$$

186 Where TP is True Positive, FP is False Positive and FN is False Negative.

### 187 3. Results

188 In this study, we created our own dataset. A large orthophoto image with a dimension of 2329x1587 was created  
 189 from UAV images. This image needs to be patched for use in the segmentation model. A python script has been  
 190 written for this purpose. It is possible to create the desired number and size of images with the written script. Random  
 191 corner coordinates with the size of 256x256 patches were created. Obtaining images with the exact corner coordinates  
 192 was prevented. Because of this condition, the program gives an error when too many images are wanted to be created.  
 193 Also, the probability of creating very similar images increases. Using the grid method, 56 images can be obtained  
 194 from the large orthophoto image. Using the random sampling method 600 images were obtained from the same image.

195 U-Net segmentation model was used with DenseNet121. IOU and F1 score values were used as metrics. Model

**Table 1**  
Model parameters

Optimizer	Adam
Learning rate	0.0001
Batch size	8
Image size	256x256
Epoch	100

196 parameters were tested with different values. The parameters and values that provide the best results are given in the  
197 table1 below.

198 IoU scores and losses graph of model is shown in Figure 6. The results of the model are satisfactory for the  
199 segmentation task. Train IoU, validation IoU, train F1-score and validation F1-score were calculated as 0.8497%,  
200 0.8461%, 0.9186%, and 0.9152%, respectively.

201 The trained model successfully detected rock blocks in the study area (Fig. 7). The boundaries of 3111 rocks of  
202 various sizes were determined and created as a vector file (.shp). This method is not recommended for smaller areas.  
203 Because sufficient training data cannot be created. In areas where there are several rock blocks, detection can also be  
204 done manually. Sometimes there may be distortions at the edges and corners of the image. This causes errors in rock  
205 block detection. Therefore, a larger area than the area where the rocks are located should be selected as the study area.

206 After the rocks were detected, each rock's volume and 3D surface area were calculated. These calculations were  
207 performed using Python. Calculated values were saved in the shape file as fill volume, cut volume and 3D area.

208 In volume calculations, there must be a reference height or surface. In this study, the heights at the boundaries  
209 of the rocks were selected as the reference height. The calculations were made using an image containing elevation  
210 data. This image consists of pixels containing elevation values. These pixels form rows and columns. The elevation  
211 values in each row were used to calculate the total volume. The polygons showing the boundaries of the rocks were  
212 masked with elevation data. Thus, data with elevation values for each rock were obtained. Volumes were calculated  
213 by proceeding along the rows. The slope was calculated by comparing the elevation values at the beginning and end  
214 of the row. A new base elevation was determined for each pixel and the volumes were calculated from this elevation.

215 In this method, it is necessary to evaluate 3 different situations. In the first case, the first height and the last height  
216 of the rows are equal. The starting elevation value is used as a reference height in this case. The volumes above this  
217 height are calculated as the fill volume, and the below are calculated as the cut volume. In the second case, the first  
218 height is greater than the last height of the rows. In the third case, the first height is less than the last height of the  
219 rows. Different calculations must be made for each situation. These situations are shown in Figure 8.

220 Volume calculation can be easily done by multiplying the pixel area by the height. Heights need to be calculated  
221 for each pixel. The starting and ending pixels along a row are assumed to be ground. These ground elevations are used

222 to find the slope, and each pixel's height is recalculated using this slope. Fill volume and cut volume were calculated  
 223 using new heights and pixel areas. Slopes, fill volumes and cut volumes were determined using the method in Figure  
 224 X. The total volumes (fill and cut) are found by summing the calculations made for each row.

225 The 3D Surface area was calculated by Python script. Calculations of flat surfaces can be found by multiplying  
 226 pixel lengths. However, different methods must be used for irregular surfaces. The gradient method was used in 3D  
 227 surface calculation. Height changes were calculated in X and Y directions, gradient vectors were obtained in each  
 228 direction. Surface areas were calculated by using these vectors. The slope correction equation is used to determine the  
 229 sloped surfaces (Equation 3).

$$\text{slope correction} = \sqrt{1 + \left(\frac{\partial z}{\partial x}\right)^2 + \left(\frac{\partial z}{\partial y}\right)^2} \quad (3)$$

$$\frac{\partial z}{\partial x} = \text{gradient in X direction}, \quad \frac{\partial z}{\partial y} = \text{gradient in Y direction}$$

The 3D surface area is calculated as following:

$$\text{3D surface area} = \text{pixel area} \times \text{slope correction}$$

## 230 4. Conclusions

231 This study aimed to segment rock blocks and calculate the volume and 3D surface areas of the blocks obtained as  
 232 a result of segmentation. The methods used in the segmentation process provided the determination of the boundaries  
 233 of rock blocks with high accuracy rates. In this way, the geometric properties of the blocks were analysed in detail.

234 U-NET deep learning network and DenseNet121 model were used as segmentation methods. The boundaries of  
 235 rock blocks were determined accurately with the trained model.

236 The volume of each rock block was successfully calculated from the data obtained after segmentation. Similarly,  
 237 the 3D surface areas of the blocks were calculated. High-resolution DEM data were used in volume and surface area  
 238 calculations. Determination of block volumes and 3D surface areas is of critical importance, especially for rockfall  
 239 simulations and engineering analyses. In addition, since the outputs of the study are coordinated vector data, they can  
 240 be easily used in any GIS software. It can be a basis for different studies and analyses.

241 This study has presented a reliable method for segmentation and volume/surface area calculations and has also

242 directly contributed to engineering applications in terms of determining the physical properties of rock masses. The  
243 segmentation section of the study is recommended for terrains containing a lot of rock blocks. It is possible to detect  
244 rock blocks in a short time. In addition, this method can be used to automatically detect different types of terrain. Deep  
245 learning models usually require a large amount of data for training. A large amount of data can be generated with the  
246 Random Sampling method proposed in this study. Volume and 3D surface area algorithms can be used not only for  
247 rock blocks but also for any object on the field. These algorithms only require precise DEM data and object boundaries.  
248 For example, these calculations can be made for a single rock block. In these calculations, ground heights and object  
249 heights must be determined clearly. When determining the object boundaries, they should be extended towards the  
250 ground. If the boundaries only represent the object, the ground heights will not be considered, and the results will not  
251 be correct. In some cases, the model can draw the boundaries of the rock blocks narrower. In this case, this problem  
252 can be solved by adding buffers to the rock blocks.

253 As a result, this study provides a basis for volumetric and geometric analyses for rock mechanics, geology and  
254 engineering applications, and can be expanded by testing on different rock types and fields in future studies.

## 255 5. Acknowledgments

256 The author wants to thank the Prime Ministry Disaster and Emergency Management Authority for supplying or-  
257 thophoto images and geological map.

258 **Code availability section**

259 Name of the code: rock\_segmentation

260 Contact: ali.polat@afad.gov.tr

261 Hardware requirements:

262 Program language: Python

263 Software required: Python v3.9

264 Program size: 35.7 KB

265 The source codes are available for downloading at the link: [https://github.com/apolat2018/rock\\_segmentation](https://github.com/apolat2018/rock_segmentation)266 **References**

- 267 Buslaev, A., Iglovikov, V.I., Khvedchenya, E., Parinov, A., Druzhinin, M., Kalinin, A.A., 2020. Albumentations: fast and flexible image augmentations. *Information* 11, 125.
- 268 Cao, Z., Liu, Z., Xu, G., Lin, H., Li, X., Nikitas, N., 2024. Risk assessment and prevention for typical railway bridge pier under rockfall impact, in: *Structures*, Elsevier. p. 106178.
- 269 Cruden, D.M., Varnes, D.J., 1996. Landslide types and processes. *Transportation Research Board, US National Academy of Sciences, Special Report* 247, 36–75.
- 270 Dunlop, H., 2006. Automatic rock detection and classification in natural scenes. *Masters Thesis, Carnegie Mellon University* .
- 271 Guo, Q., Wang, Y., Yang, S., Xiang, Z., 2022. A method of blasted rock image segmentation based on improved watershed algorithm. *Scientific Reports* 12, 7143.
- 272 Hutchinson, J., 1988. Morphological and geotechnical parameters of landslides in relation to geology and hydrogeology, landslides, in: *Proceedings of the fifth international symposium on landslides*, pp. 3–35.
- 273 Jaccard, P., 1912. The distribution of the flora in the alpine zone. 1. *New phytologist* 11, 37–50.
- 274 Ji, Z.M., Chen, T.L., Wu, F.Q., Li, Z.H., Niu, Q.H., Wang, K.Y., 2023. Assessment and prevention on the potential rockfall hazard of high-steep rock slope: a case study of zhongyuntai mountain in lianyungang, china. *Natural Hazards* 115, 2117–2139.
- 275 Kainthola, A., Pandey, V.H.R., Singh, P., Singh, T., 2023. Stability assessment of markundi hills using q-slope, smr and simulation tools, in: *Landslides: Detection, Prediction and Monitoring: Technological Developments*. Springer, pp. 87–107.
- 276 Karimpouli, S., Tahmasebi, P., 2019. Segmentation of digital rock images using deep convolutional autoencoder networks. *Computers & geosciences* 126, 142–150.
- 277 Keskin, İ., Polat, A., 2022. Kinematic analysis and rockfall assessment of rock slope at the unesco world heritage city (safranbolu/turkey). *Iranian Journal of Science and Technology, Transactions of Civil Engineering* 46, 367–384.
- 278 Kuang, B., Wisniewski, M., Rana, Z.A., Zhao, Y., 2021. Rock segmentation in the navigation vision of the planetary rovers. *Mathematics* 9, 3048.
- 279 Liu, W.l., Dong, J.x., Xu, H.h., Sui, S.g., Yang, R.x., Zhou, L.s., 2021. Trajectory analysis and risk evaluation of dangerous rock mass instability of an overhang slope, southwest of china. *Advances in civil engineering* 2021, 7153535.
- 280 Malladi, S.R.S., Ram, S., Rodríguez, J.J., 2014. Superpixels using morphology for rock image segmentation, in: *2014 Southwest Symposium on Image Analysis and Interpretation, IEEE*. pp. 145–148.
- 281 Ronneberger, O., Fischer, P., Brox, T., 2015. U-net: Convolutional networks for biomedical image segmentation, in: *Medical image computing and*

Short title

- 293 computer-assisted intervention–MICCAI 2015: 18th international conference, Munich, Germany, October 5-9, 2015, proceedings, part III 18,  
294 Springer. pp. 234–241.
- 295 Song, Y., Shan, J., 2006. A framework for automated rock segmentation of the mars exploration rover imagery. URL: <https://api.semanticscholar.org/CorpusID:39798752>.
- 296
- 297 Varnes, D., 1978. Slope movement types and processes. *Landslides: analysis and control* .
- 298 Xue, Z., Chen, L., Liu, Z., Lin, F., Mao, W., 2021. Rock segmentation visual system for assisting driving in tbm construction. *Machine Vision and*  
299 *Applications* 32, 77.
- 300 Yılmaz, H., Yılmaz, A., 2004. Divriği (sivas) yöresinin jeolojisi ve yapısal evrimi. *Türkiye Jeoloji Bülteni* 47, 13–46.

**301 List of Figures**

302 1	Location map . . . . .	12
303 2	Geological map (1/25000 scale geological map of General Directorate of Mineral Research and Ex- 304 plorations) (a), rock blocks (b), settlement and rocks (c) . . . . .	13
305 3	Workflow diagram . . . . .	14
306 4	Train and test sampling areas. 1,5,9 test sampling area and 2,3,4,6,7,8 train sampling area . . . . .	15
307 5	U-Net architecture . . . . .	16
308 6	DenseNet121 IoU and Loss values . . . . .	17
309 7	Result map of the model (a) original view, (b,c,d )zoomed views. . . . .	18
310 8	Volume calculation methods. (a) first height is greater than the last height of the rows,(b) b) first height 311 is less than the last height of the rows . . . . .	19

Short title

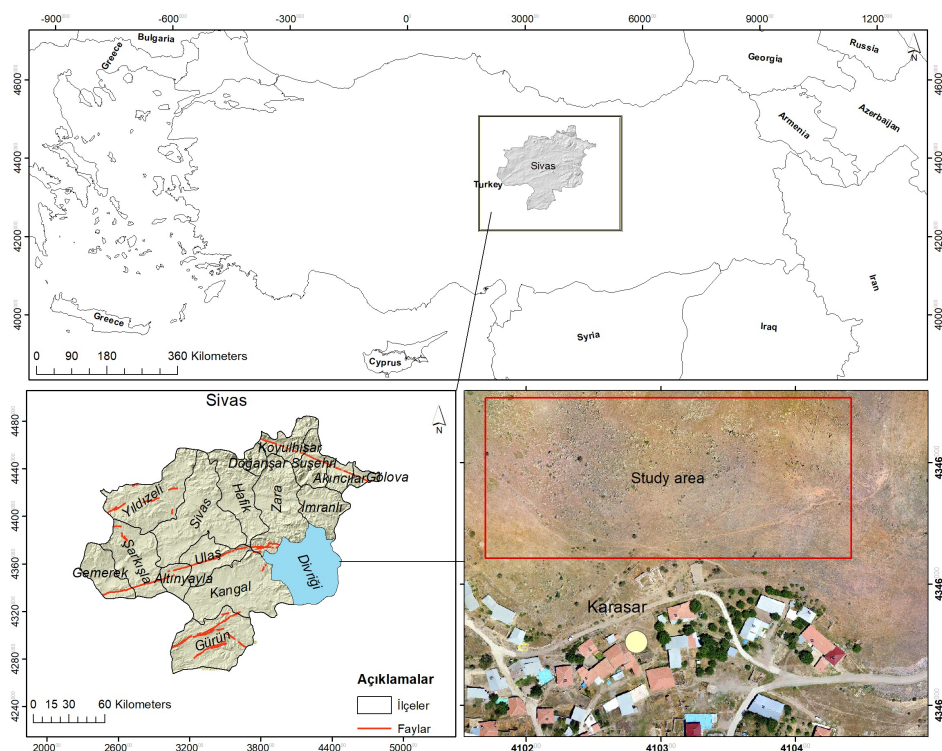
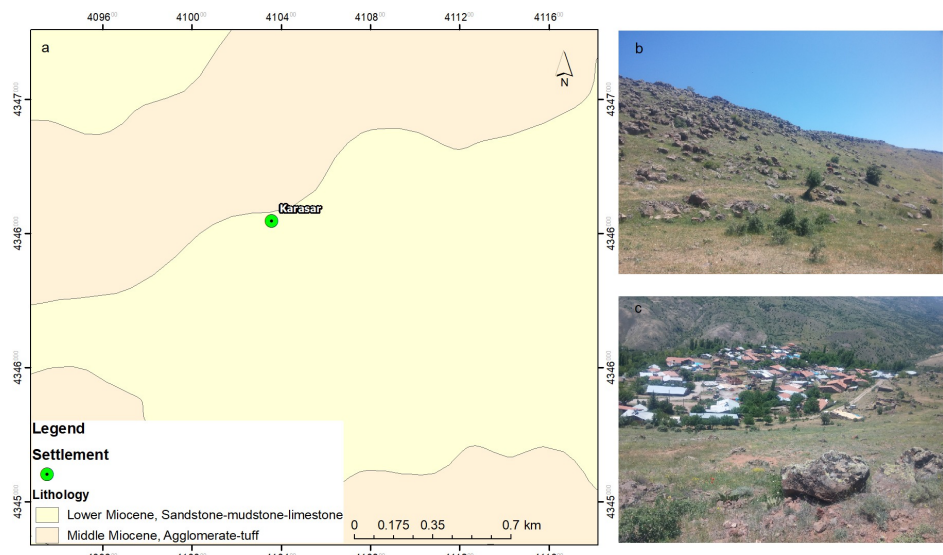


Figure 1: Location map



**Figure 2:** Geological map (1/25000 scale geological map of General Directorate of Mineral Research and Explorations (a), rock blocks (b), settlement and rocks (c)

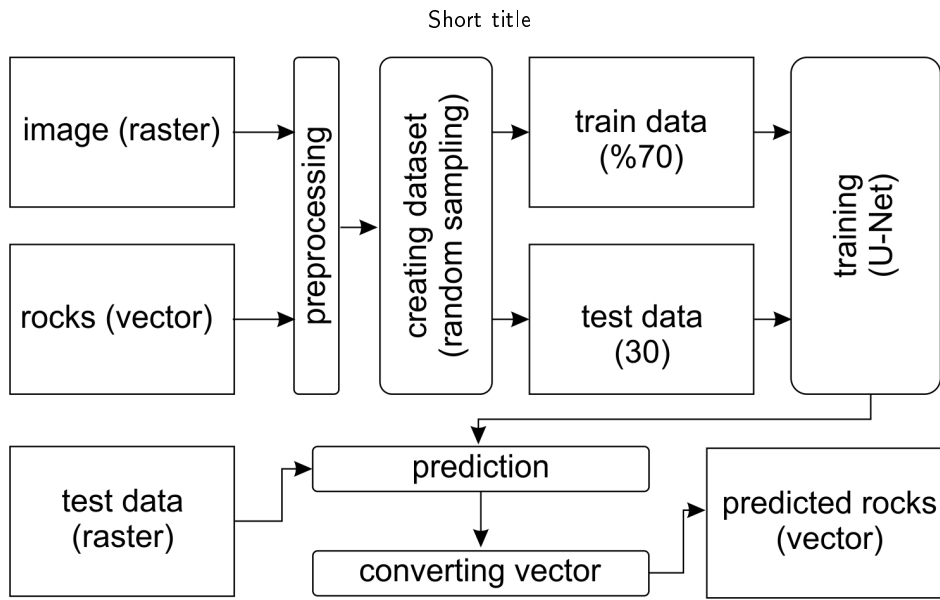
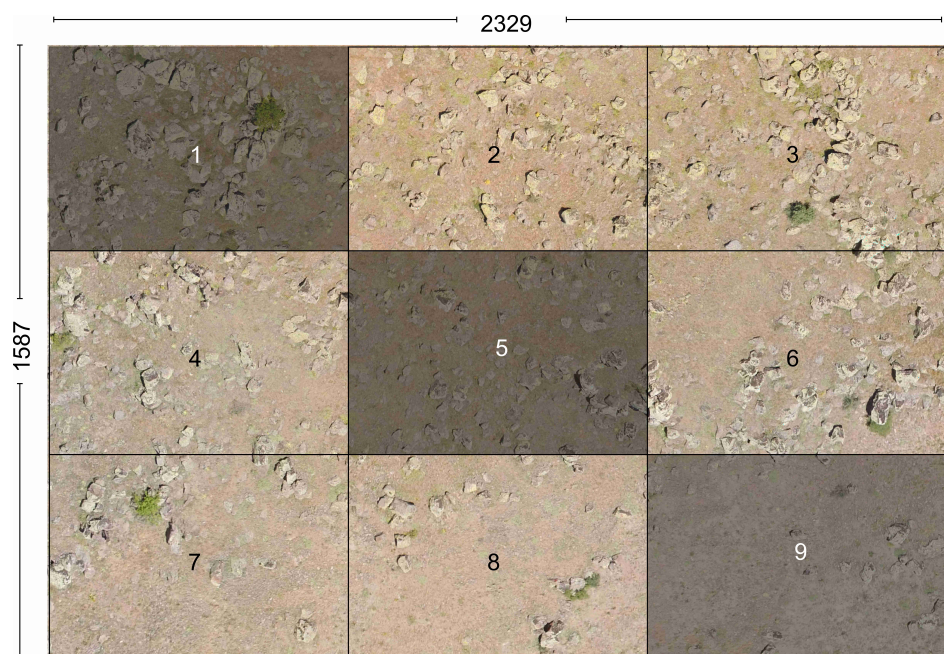
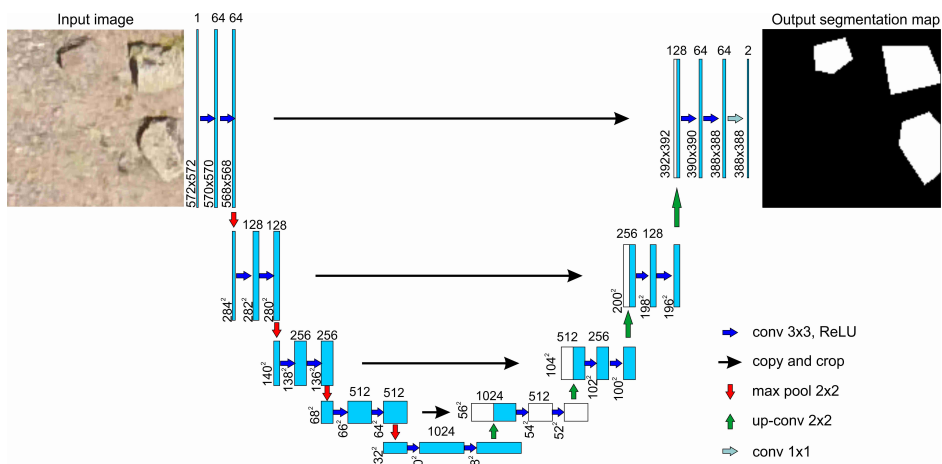


Figure 3: Workflow diagram



**Figure 4:** Train and test sampling areas. 1,5,9 test sampling area and 2,3,4,6,7,8 train sampling area

### Short title



**Figure 5:** U-Net architecture

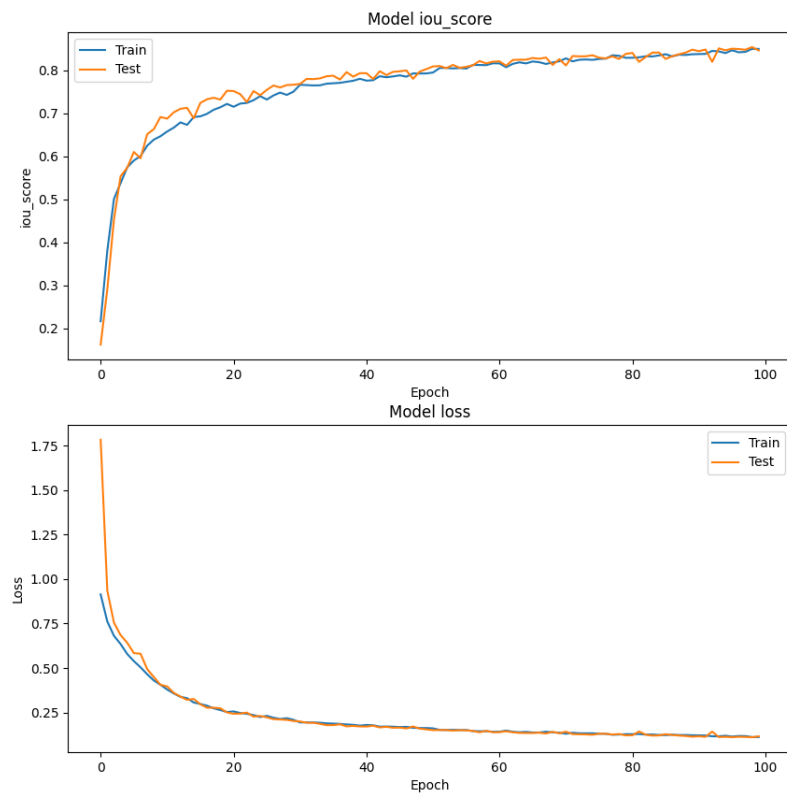


**Figure 6:** DenseNet121 IoU and Loss values

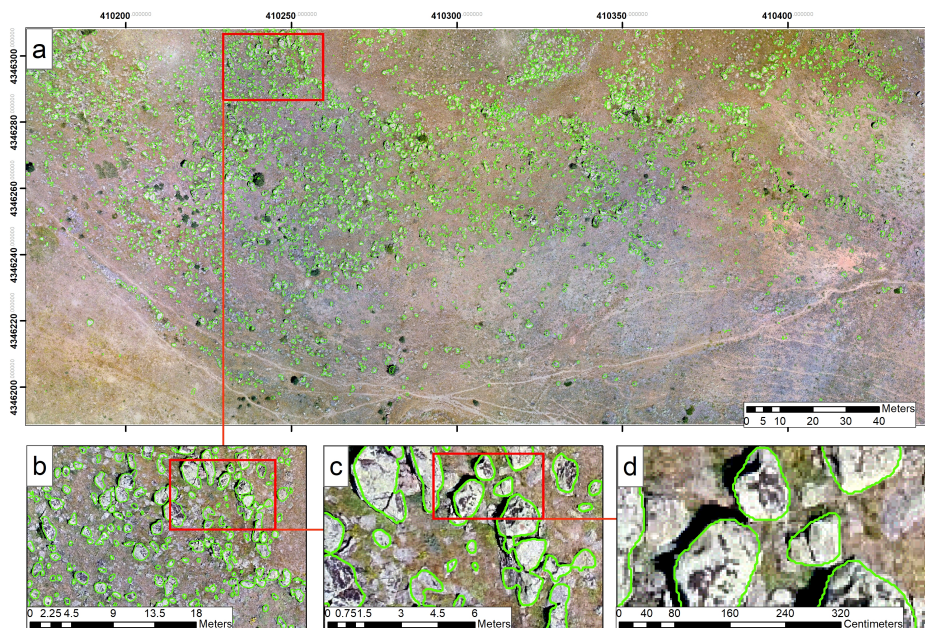


**Figure 7:** Result map of the model (a) original view, (b,c,d )zoomed views.

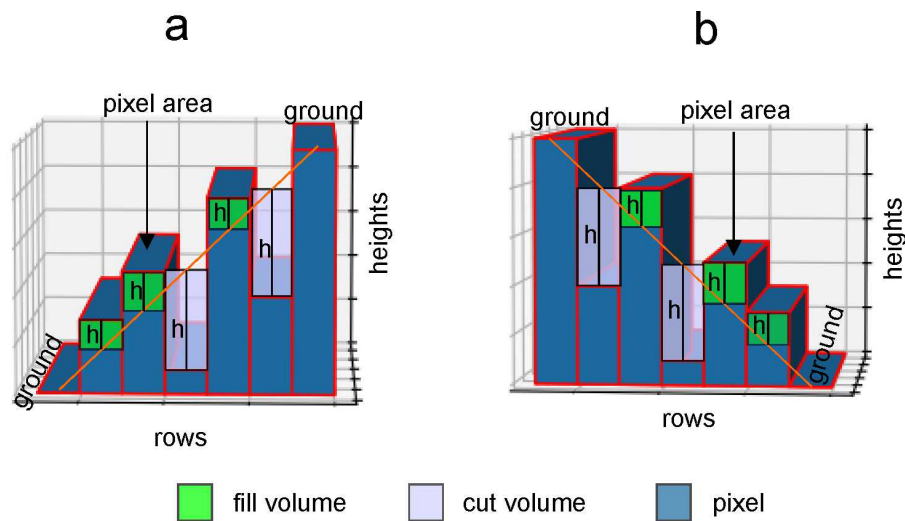


**Figure 8:** Volume calculation methods. (a) first height is greater than the last height of the rows,(b) b) first height is less than the last height of the rows